Supporting Information

Supramolecular Assemblies of Tetravalent Terbium Complex Units: Syntheses, Structure, and Materials Properties

Tianjiao Xue, [a, b] *Qing-Song Yang,* [a,b] *Lei Li,* [a,b] *Xiao-Yong Chang,* [a] *You-Song Ding*,* [a,b] *and Zhiping Zheng** [a, b]

[a] *Department of Chemistry, Southern University of Science and Technology, Shenzhen, Guangdong 518055, China.*

[b] *Key University Laboratory of Rare Earth Chemistry of Guangdong, Southern University of Science and Technology, Shenzhen, Guangdong 518055.*

**Corresponding authors: dingys@sustech.edu.cn; zhengzp@sustech.edu.cn.*

Contents

Table S1. Reaction conditions for the oxidation of Tb(III)/Pr(III)/Pr(IV) complexes to Tb(IV)/Pr(IV)/Pr(V) complexes.

Ln(III/IV) precursor	Additive	Oxidant	Ln(IV/V) complex	Neutral ligand	Stability	Ref
$[KTb(L^{OtBu})_4]$	-	[OX]1	$[Tb(L^{OtBu})_4]$	-	in argon	[1]
$[(Et_2O)K][Tb(L^{NP*})_4]$	-	AgI	$[Tb(L^{NP*})_4]$	-	in argon	[2]
$[KTb(L^{Ph})_4(THF)]$	-	[OX]1 [OX]2	$[Tb(L^{Ph})_4(MeCN)_2]$ $[Tb(L^{Ph})_4(THF)_2]$ $[Tb(L^{Ph})_4(OPR_3)]$	MeCN THF OPR_3 (R=Ph, Et)	80% left for 96 h in tol	[3, 4]
$[K(tol)\{Tb(L^{Ar})(L^{Ph})\}]$		[OX]1	$[Tb(L^{Ar})(L^{Ph})(MeCN)_2]$	MeCN	82% left for 48 h in tol	[5]
$Tb(L^{Ph})_3(THF)_3$	KL^{Ph}	[OX]1	$[Tb(L^{Ph})_4L]$	L=DME, bpy, bpym, phen	49 % left for 5 days in tol	[6]
$[KPr(L^{Ph})_4(THF)]$	-	[OX]1	$[Pr(L^{Ph})_4(MeCN)_2]$ $[Pr(L^{Ph})_4(MeCN)(OPPh_3)]$	MeCN $OPPh_3$	80% left for 24 h in tol	[4, 7]
$[(Et_2O)K][Pr(L^{NP*})_4]$	-	AgI	$[Pr(L^{NP*})_4]$	-	survive at -35°C	[8]
$PrI_3(THF)_4$	HL^{NP}; KBn	AgI	$[Pr(L^{NP})_4]$	-	99% left for 24 h in THF-d_8	[9]
$Pr(L^{Ph})_3(THF)_3$	KL^{Ph}	[OX]1	$[Pr(L^{Ph}{}_3)_4bpyOMe]$	bpyOMe	57 % left for 7 days in tol	[10]
$[Pr(L^{NP})_4]$	-	[OX]3 [OX]4	$[Pr^{V}(L^{NP})_4][BArF_{20}]$ $[Pr^{V}(L^{NP})_4][PF_6]$	-	stable at -30°C in THF-d_8	[11]
$Tb(L^{Ph})_3(THF)_3$	KL^{Ph}	$TABF_4$	$[Tb(L^{Ph})_4L]_n$	L=L1-L5	in air for 2 days	This work

L^{OtBu} = $OSi(OtBu)_3$; L^{NP*} = NP(1,2-bis-*t*Bu-diamidoethane)(NEt_2); L^{NP} = NP^tBu_3; L^{Ph} = $OSiPh_3$; L^{Ar} = $(OSiPh_2Ar)_3$-arene; bpy = 2,2'-bipyridine; bpym = 2,2'-bipyrimidine; phen = 1,10-phenanthroline; bpyOMe = 4,4'-dimethoxy-2,2'-bipyridine;

[OX]1 = $[N(C_6H_4Br)_3][SbCl_6]$; [OX]2 = $[N(C_6H_4Br)_3][OTf]$; [OX]3 = $[Fc][BArF_{20}]$; [OX]4 = $[Ag][PF_6]$; $TABF_4$ = thianthrene cation radical tetrafluoroborate

1. Experimental Section

General Considerations and Methods. All manipulations were carried out with standard Schlenk techniques or in a glovebox under an argon atmosphere. Glassware was dried overnight at 120 °C before use. Toluene and n-hexane were dried over activated alumina and stored over potassium mirror before use. All other reagents including solvents were purchased from Energy-Chemical and used without further purification. Anhydrous $TbCl_3$ [12], $Tb(OSiPh_3)_3(THF)_3$ [13] and $TABF_4$ [14] were synthesized by adopting the literature procedures. Elemental analyses were recorded on a Carlo Erba EA1110 simultaneous CHN elemental analyzer. Powder X-ray diffraction (PXRD) data were collected in the range of $5° \leq 2\theta \leq 50°$ at room temperature against the bulk samples on a Rigaku SmartLab 9KW diffractometer with Cu Kα radiation in a flat silicon plate. The UV–Vis–NIR absorbance spectra were recorded at room temperature on a UV-3600i Plus spectrophotometer (SHIMADZU) with $BaSO_4$ as the reference material. Fourier transform infrared (FTIR) spectra were collected on a Bruker Alfa spectrophotometer in the range of 600–4000 cm^{-1}.

$[Tb(OSiPh_3)_4$(1,2-bis(4-pyridyl)ethane)$]_2$ (1). A solution of $TABF_4$ (0.03 g, 0.1 mmol, 1 equiv.) in MeCN (2 mL) was added at room temperature to a slurry solution of $Tb(OSiPh_3)_3(THF)_3$ (0.12 g, 0.1 mmol, 1 equiv.) and $KOSiPh_3$ (0.03 g, 0.1 mmol, 1 equiv.) in MeCN (1 mL). The nearly colorless suspension changed to magenta immediately. After stirring for 10 min, bright orange precipitates were formed in a pale yellow supernatant. The orange solid was filtered and washed with 1 mL MeCN for three times. A colorless solution of 1,2-bis(4-pyridyl)ethane (0.022 g, 0.1 mmol, 1

equiv.) in toluene (5 mL) was added at room temperature to the orange solid. The residue was extracted with toluene solution and the red-orange solution was filtered. Dark red octahedron-shaped single crystals suitable for X-ray diffraction analysis were obtained upon overnight standing at room-temperature of the filtrate (80 mg, 46% yield). IR: ν [cm^{-1}] = 3045 (w), 2995 (w), 2360 (m), 2339 (m), 1615 (w), 1427 (m), 1111 (m), 1066 (w), 910 (s), 819 (w), 743 (w), 699 (s). Anal. Calc. for $[Tb(OSiPh_3)_4(L1)]_2$ (2865.47 g mol^{-1}): $C_{168}H_{144}N_4O_8Si_8Tb_2$: C, 70.41; H, 5.07; N, 1.95. Found: C, 70.15; H, 5.16; N, 2.06.

$[Tb(OSiPh_3)_4$(4,4'-bipyridine)$]_n$ (2). As described for **1**, an orange solid was obtained by a mixture of $Tb(OSiPh_3)_3(THF)_3$, $KOSiPh_3$ and $TABF_4$ in 3 mL MeCN. A colorless solution of 4,4'-bipyridine (0.02 g, 0.1 mmol, 1 equiv.) in toluene (5 mL) was added at room temperature to the orange solid. The residue was extracted with toluene solution and the orange-red solution was filtered. Orange needle-like single crystals suitable for X-ray diffraction analysis were obtained upon overnight standing at room-temperature of the filtrate (93 mg, 56% yield). IR: ν [cm^{-1}] = 3054 (w), 3020 (w), 1963 (w), 1893 (w), 1824 (w), 1774 (w), 1604 (w), 1531 (w), 1484 (w), 1427 (m), 1184 (w), 1110 (s), 1029 (w), 998 (w), 910 (s), 806 (w), 740 (m), 710 (s), 624 (m). Anal. Calc. for $[Tb(OSiPh_3)_4(L2)]_n$ (1620.99 g mol^{-1}): $C_{99.5}H_{88}N_2O_4Si_4Tb$: C, 69.52; H, 4.84; N, 1.98. Found: C, 69.49; H, 5.01; N, 2.35.

$[Tb(OSiPh_3)_4$(1,2-bis(4-pyridyl)acetylene$)]_n$ (3). As described for **1**, an orange solid was obtained by a mixture of $Tb(OSiPh_3)_3(THF)_3$, $KOSiPh_3$ and $TABF_4$ in 3 mL MeCN. A colorless solution of 1,2-bis(4-pyridyl)ethylene (0.018 g, 0.1 mmol, 1

equiv.) in toluene (5 mL) was added at room temperature to the orange solid. The residue was extracted with toluene solution and the orange-red solution was filtered. Red plate-shaped single crystals suitable for X-ray diffraction analysis were obtained upon overnight standing at room-temperature of the filtrate (68 mg, 39% yield). IR: ν [cm^{-1}] = 3043 (w), 2993 (w), 2908 (w), 1963 (w), 1893 (w), 1828 (w), 1778 (w), 1608 (m), 1427 (m), 1110 (m), 914 (s), 740 (w), 701 (s), 609 (w). Anal. Calc. for $[Tb(OSiPh_3)_4(L3)]_n$ (1719.14 g mol^{-1}): $C_{105}H_{94}N_2O_4Si_4Tb$: C, 69.93; H, 4.89; N, 1.94. Found: C, 70.28; H, 5.266; N, 2.25.

$[Tb(OSiPh_3)_4$(1,2-bis(4-pyridyl)ethylene)$]_n$ (4). As described for **1**, an orange solid was obtained by a mixture of $Tb(OSiPh_3)_3(THF)_3$, $KOSiPh_3$ and $TABF_4$ in 3 mL MeCN. A colorless solution of 1,2-bis(4-pyridyl)acetylene (0.018 g, 0.1 mmol, 1 equiv.) in toluene (5 mL) was added at room temperature to the orange solid. The residue was extracted with toluene solution and the orange-red solution was filtered. Red plate-shaped single crystals suitable for X-ray diffraction analysis were obtained upon overnight standing at room-temperature of the filtrate (85 mg, 50% yield). IR: ν [cm^{-1}] = 3047 (w), 2996 (w), 2908 (w), 1963 (w), 1893 (w), 1828 (w), 1774 (w), 1608 (m), 1484 (w), 1427 (m), 1257 (w), 1218 (w), 1184 (w), 1110 (m), 1037 (w), 1010 (w), 910 (s), 825 (w), 736 (w), 698 (s), 613 (w). Anal. Calc. for $[Tb(OSiPh_3)_4(L4)]_n$ (1717.13 g mol^{-1}): $C_{105}H_{92}N_2O_4Si_4Tb$: C, 70.03; H, 4.76; N, 1.94. Found: C, 70.26; H, 5.155; N, 1.90.

$[Tb(OSiPh_3)_4$(1,4-bis(4-pyridyl)benzene)$]_n$ (5). As described for **1**, orange solid was obtained by a mixture of $Tb(OSiPh_3)_3(THF)_3$, $KOSiPh_3$ and $TABF_4$ in 3 mL

MeCN. The residue was extracted with 3 mL ethylene glycol dimethyl ether (DME), and the red-orange solution was filtered. A colorless solution of 1,4-bis(4-pyridyl)benzene (0.022 g, 0.1 mmol, 1 equiv.) in DME (2 mL) was layered to the orange-red solution at room temperature. Red block-shaped single crystals suitable for X-ray diffraction analysis were obtained overnight (63 mg, 34% yield). IR: ν [cm^{-1}] = 3667 (w), 2985 (w), 2900 (w), 1963 (w), 1897 (w), 1828 (w), 1608 (w), 1484 (w), 1427 (w), 1253 (w), 1222 (w), 1187 (w), 1106 (m), 1068 (w), 1037 (w), 1006 (w), 910 (s), 809 (w), 740 (w), 701 (s), 609 (w). Anal. Calc. for $[Tb(OSiPh_3)_4(L5)]_n$ (1853.27 g mol^{-1}): $C_{104}H_{112}N_2O_{12}Si_4Tb$: C, 70.80; H, 4.86; N, 1.87. Found: C, 69.12; H, 4.319; N, 2.59.

2. Crystallographic Data

Suitable single crystals of compounds **1**-**5** were embedded in protective perfluoropolyalkyether oil (viscosity 1800 cSt; ABCR GmbH) on a microscope slide and a single specimen (Dark red octahedron shape single crystal 0.05 × 0.05 × 0.05 mm^3 for **1**; orange needle shape single crystal 0.03 × 0.01 × 0.01 mm^3 for **2**; red plate shape single crystal 0.34 × 0.26 × 0.03 mm^3 for **3**; red plate shape single crystal 0.1 × 0.1 × 0.03 mm^3 for **4**; red block shape single crystal 0.05 × 0.05 × 0.05 mm^3 for **5**) was selected and subsequently transferred to the cold nitrogen gas stream of the diffractometer.

Single-crystal X-ray diffraction data were collected on a diffractometer with Mo-Kα radiation at T = 100 K for **1**. The maximum resolution achieved was 0.77 Å.

Single-crystal X-ray diffraction data were collected on a diffractometer with Ga-Kα radiation at T = 100 K for **2**. The maximum resolution achieved was 0.84 Å.

Single-crystal X-ray diffraction data were collected on a diffractometer with Ga-Kα radiation at T = 200 K for **3**. The maximum resolution achieved was 0.83 Å. The crystal exhibits two twin domains; however, the data obtained from one domain is of superior quality compared to that from the other domains. Consequently, the detwinned HKLF 4 data, acquired after splitting diffraction spots using the APEX3 program, was utilized for analyzing the molecular structure [15]. The Solvent Mask [16] routine of the Olex2 software was implemented to remove the contributions of four disordered toluene solvent to the observed structure factors. The entire two 1,2-bis(4-pyridyl)ethylene were disordered. N1, N2, C73-C82, C155, C156 and N1A, N2A, C73A-C82A, C170, C1L were disordered over two sites with occupancies 0.649:0.351. N3, N4, C157-C168 and N3A, N4A, C1A-C1K, C169 were disordered over two sites with occupancies 0.640:0.360.

Single-crystal X-ray diffraction data were collected on a diffractometer with Ga-Kα radiation at T = 100 K for **4**. The maximum resolution achieved was 0.82 Å. The crystal exhibits two twin domains; however, the data obtained from one domain is of superior quality compared to that from the other domains. Consequently, the detwinned HKLF 4 data, acquired after splitting diffraction spots using the APEX3 program, was utilized for analyzing the molecular structure [15].

Single-crystal X-ray diffraction data were collected on a diffractometer with Mo-Kα radiation at T = 100 K for **5**. The maximum resolution achieved was 0.77 Å.

The phenyl in the 1,4-bis(4-pyridyl)benzene was disordered which C13, C53 and C5, C21 disordered over two sites with occupancies 0.462:0.538. The two DME solvent molecules were disordered. O11, O45, C3, C23, C25, C47 and O11A, O45A, C3A, C23A, C25A, C47A disordered over two sites with occupancies 0.5:0.5; O46, O47, C55-C58 and O46A, O47A, C55A-C58A disordered over two sites with occupancies 0.462:0.538.

Using Olex2 [17], the structures were solved with the SHELXT structure solution program using Intrinsic Phasing [18] and refined with the SHELXL refinement package using Least Squares minimization [19]. All hydrogen atom positions were generated geometrically and refined with isotropic temperature factors. Cambridge Crystallographic Data Centre contains the crystal structure with the following CCDC number 2410273 (**1**), 2337622 (**2**), 2351767 (**3**), 2351768 (**4**) and 2337623 (**5**).

Table S2. Collection of Crystallographic Data of **1-5**.

	1	**2**	**3**	**4**	**5**
Formula	$C_{200}H_{208}N_4O_{16}Si_8Tb_2$	$C_{99.5}H_{88}N_2O_4Si_4Tb$	$C_{210}H_{188}N_4O_8Si_8Tb_2$	$C_{105}H_{92}N_2O_4Si_4Tb$	$C_{104}H_{112}N_2O_{12}Si_4Tb$
F.w.	3410.46	1645.99	3438.19	1717.08	1853.23
T (K)	99.9	100.0	200.0	100.0	100.0
cell	orthorhombic	triclinic	triclinic	triclinic	monoclinic
Space group	*Fddd*	*P*-1	*P*-1	*P*-1	*C*2/*c*
a (Å)	32.2780(17)	17.3266(11)	17.8325(16)	17.7840(16)	22.7842(9)
b (Å)	34.1126(16)	23.1849(15)	21.184(2)	21.250(2)	18.3307(7)
c (Å)	39.4068(17)	24.3639(14)	25.671(2)	25.315(3)	23.9399(8)
α (°)	90	93.487(3)	109.037(4)	109.025(4)	90
β (°)	90	110.590(3)	101.480(3)	101.840(4)	111.8750(10)
γ (°)	90	109.064(4)	90.122(3)	90.039(4)	90
V (Å^3)	43390(4)	8487.2(9)	8960.2(14)	8828.1(15)	9278.6(6)
Z	8	4	2	4	4
F(000)	15088.0	3408.0	3564.0	3556.0	3868.0
D_c (g cm^{-3})	1.105	1.289	1.274	1.292	1.327
μ (mm^{-1})	0.746	4.941	4.694	4.765	0.877
Data collected/unique	173686/12500	168101/30012	32561/32561	31807/31807	49787/10686
$R1$ (>2σ/all data)	0.0514/0.0609	0.0635/0.0895	0.0600/0.0732	0.0800/0.1940	0.0442/0.0543
wR2 (>2σ/all data)	0.1505/0.1600	0.1621/0.1767	0.1757/0.1856	0.1250/0.2201	0.1066/0.1164
GOF	1.142	1.082	1.159	1.093	1.034
Residues (e Å^{-3})	1.30/-0.83	1.00/-1.07	1.79/-1.60	1.77/-1.15	1.13/-0.78

Table S3. Continuous Shape Measures (CShM) calculations [20] for **1-5**.

Structure [ML6][a]	HP-6	PPY-6	OC-6	TPR-6	JPPY-6
1	33.032	28.509	0.566	16.265	31.614
2-Tb1	32.710	24.441	1.148	13.554	27.394
2-Tb2	32.209	24.266	1.133	13.297	27.331
3-Tb1	33.093	25.146	0.940	13.802	28.245
3-Tb2	33.009	25.463	0.849	14.034	28.556
4-Tb1	33.091	25.709	0.920	14.457	28.716
4-Tb2	33.111	26.177	0.798	14.482	29.210
5	32.941	27.323	0.675	15.542	30.410

[a] HP-6 = Hexagon (D_{6h}); PPY-6 = Pentagonal pyramid (C_{5v}); OC-6 = Octahedron (O_h); TPR-6 = Trigonal prism (D_{3h}); JPPY-6 = Johnson pentagonal pyramid J2 (C_{5v})

Table S4. Selected bond lengths (Å) and angles (°) for Tb ions in **1-5.**

Complex	Tb-X bond length (Å)		X-Tb-X angle(°)					
1	Tb1-O1	2.046(3)	O1- Tb1- O1[a]	100.92(16)	O2[a]- Tb1- O1	96.68(10)	O2- Tb1- N1[d]	82.58(10)
	Tb1-O1[a]	2.046(3)	O1[a]- Tb1- N1	89.75(11)	O2- Tb1- O1	96.62(10)	O2- Tb1- N1	81.35(10)
	Tb1-O2	2.075(2)	O1- Tb1- N1[a]	89.75(11)	O2- Tb1- O1[a]	96.68(10)	N1[a]- Tb1- N1	79.58(14)
	Tb1-O2[a]	2.075(2)	O1- Tb1- N1	169.31(11)	O2[a]- Tb1- O2	159.03(15)		
	Tb1-N1	2.484(3)	O1[a]- Tb1- N1[a]	169.30(11)	O2[a]- Tb1- N1[a]	81.34(10)		
	Tb1-N1[a]	2.484(3)	O2[a]- Tb1- O1[a]	96.62(10)	O2[a]- Tb1- N1	82.58(9)		
2	Tb1-O1	2.064(4)	O1- Tb1- O4	99.20(16)	O3- Tb1- N2	175.41(17)	O5- Tb2- N1[b]	79.72(15)
	Tb1-O2	2.055(4)	O1- Tb1- N2	84.92(16)	O3- Tb1- N3	88.51(17)	O6- Tb2- O8	98.31(16)
	Tb1-O3	2.041(4)	O1- Tb1- N3	171.80(16)	N3- Tb1- N2	86.90(17)	O6- Tb2- O5	100.14(16)
	Tb1-O4	2.083(4)	O4- Tb1- N2	79.84(16)	O8- Tb2- O5	152.41(16)	O6- Tb2- N4	172.15(16)
	Tb1-N2	2.536(5)	O4- Tb1- N3	78.68(17)	O8- Tb2- N4	80.75(16)	O6- Tb2- N1[b]	84.09(16)
	Tb1-N3	2.501(5)	O2- Tb1- O1	100.06(17)	O8- Tb2- N1[b]	81.97(15)	N4- Tb2- N1[b]	88.07(16)
	Tb2-O5	2.080(4)	O2- Tb1- O4	151.44(16)	O7- Tb2- O8	99.81(15)		
	Tb2-O6	2.053(4)	O2- Tb1- N2	81.07(16)	O7- Tb2- O5	96.99(16)		
	Tb2-O7	2.051(4)	O2- Tb1- N3	79.26(17)	O7- Tb2- O6	100.02(16)		
	Tb2-O8	2.073(4)	O3- Tb1- O1	99.67(17)	O7- Tb2- N4	87.81(16)		
	Tb2-N1[b]	2.541(5)	O3- Tb1- O4	99.39(17)	O7- Tb2- N1[b]	175.18(15)		
	Tb2-N4	2.499(5)	O3- Tb1- O2	97.94(17)	O5- Tb2- N4	78.17(16)		
3	Tb1-O1	2.048(3)	O1- Tb1- O3	96.95(12)	O4- Tb1- N1	80.6(6)	O7- Tb2- N2	172.8(4)
	Tb1-O2	2.036(3)	O1- Tb1- O4	99.23(12)	O4- Tb1- N3	81.0(9)	O7- Tb2- N4[c]	83.6(3)
	Tb1-O3	2.089(3)	O1- Tb1- N1	84.9(5)	N3- Tb1- N1	88.0(7)	O8- Tb2- O6	155.05(12)
	Tb1-O4	2.077(3)	O1- Tb1- N3	172.7(5)	O5- Tb2- O6	98.21(12)	O8- Tb2- N2	80.8(6)
	Tb1-N1	2.532(7)	O2- Tb1- O1	98.24(12)	O5- Tb2- O7	97.81(12)	O8- Tb2- O4	81.2(4)
	Tb1-N3	2.522(11)	O2- Tb1- O3	98.03(12)	O5- Tb2- O8	98.09(11)	N2- Tb2- N4[c]	89.4(5)

	Tb2-O5	2.032(3)	O2- Tb1- O4	98.36(12)	O5- Tb2- N2	89.3(4)		
	Tb2-O6	2.090(3)	O2- Tb1- N1	176.9(4)	O5- Tb2- N4[c]	178.5(3)		
	Tb2-O7	2.041(3)	O2- Tb1- N3	88.9(5)	O6- Tb2- N2	80.6(6)		
	Tb2-O8	2.066(3)	O3- Tb1- N1	82.0(6)	O6- Tb2- N4[c]	82.1(4)		
	Tb2-N2	2.519(7)	O3- Tb1- N3	80.6(8)	O7- Tb2- O6	97.14(12)		
	Tb2-N4[c]	2.518(12)	O4- Tb1- O3	155.01(13)	O7- Tb2- O8	99.21(12)		
4	Tb1-O1	2.024(6)	O1- Tb1- O2	99.0(2)	O4- Tb1- N1	82.7(2)	O7- Tb2- N2	169.5(2)
	Tb1-O2	2.056(5)	O1- Tb1- O3	98.6(2)	O4- Tb1- N4[d]	79.8(2)	O7- Tb2- N3	86.9(2)
	Tb1-O3	2.046(5)	O1- Tb1- O4	98.2(2)	N1- Tb1- N4[d]	83.9(2)	O8- Tb2- O6	155.1(2)
	Tb1-O4	2.073(5)	O1- Tb1- N1	173.7(2)	O5- Tb2- O6	97.6(2)	O8- Tb2- N2	81.3(2)
	Tb1-N1	2.548(7)	O1- Tb1- N4[d]	90.2(2)	O5- Tb2- O7	99.2(2)	O8- Tb2- N3	79.8(2)
	Tb1-N4[d]	2.519(7)	O2- Tb1- O4	154.1(2)	O5- Tb2- O8	99.0(2)	N3- Tb2- N2	82.7(2)
	Tb2-O5	2.024(5)	O2- Tb1- N1	78.2(2)	O5- Tb2- N2	90.5(2)		
	Tb2-O6	2.089(5)	O2- Tb1- N4[d]	81.0(2)	O5- Tb2- N3	173.2(2)		
	Tb2-O7	2.034(5)	O3- Tb1- O2	99.5(2)	O6- Tb2- N2	80.1(2)		
	Tb2-O8	2.066(5)	O3- Tb1- O4	96.8(2)	O6- Tb2- N3	81.6(2)		
	Tb2-N2	2.506(7)	O3- Tb1- N1	87.4(2)	O7- Tb2- O6	96.9(2)		
	Tb2-N3	2.537(7)	O3- Tb1- N4[d]	171.0(2)	O7- Tb2- O8	98.4(2)		
5	Tb1-O1	2.078(2)	O1- Tb1- O1[e]	156.63(13)	O2[e]- Tb1- O1	96.88(9)	O2- Tb1- N1[e]	88.98(9)
	Tb1-O1[e]	2.078(2)	O1[e]- Tb1- N1	82.56(9)	O2- Tb1- O1	98.03(9)	O2- Tb1- N1	170.62(9)
	Tb1-O2	2.048(2)	O1- Tb1- N1[e]	82.56(9)	O2- Tb1- O1[e]	96.88(9)	N1[e]- Tb1- N1	81.69(12)
	Tb1-O2[e]	2.047(3)	O1- Tb1- N1	79.81(9)	O2[e]- Tb1- O2	100.35(13)		
	Tb1-N1	2.492(3)	O1[e]- Tb1- N1[e]	79.81(9)	O2[e]- Tb1- N1[e]	170.62(9)		
	Tb1-N1[e]	2.492(3)	O2[e]- Tb1- O1[e]	98.03(9)	O2[e]- Tb1- N1	88.98(9)		

[a] +X,3/4-Y,3/4-Z; [b] -1+X,+Y,+Z; [c] +X,1+Y,+Z; [d] +X,-1+Y,+Z; [e] 1-X,+Y,1/2-Z;

3. π-π stacking interactions

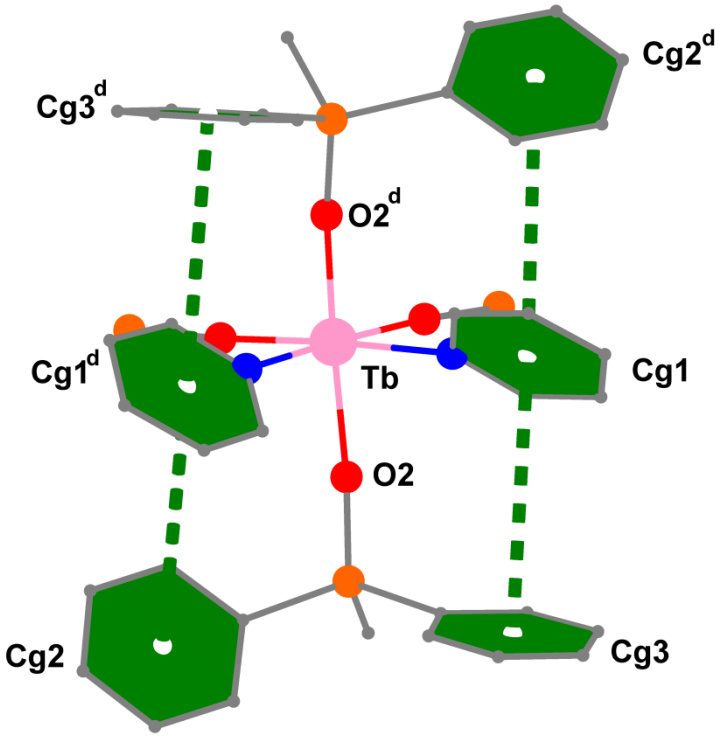

Figure S1 π-π interactions of complex **1**. Color code: pink (Tb), red (O), orange (Si), gray (C), blue (N), black (H).

d +X,3/4-Y,3/4-Z

Table S5. π-π stacking interactions in **1** (distance (Å), angles: (°))**.** Cg-Cg: Distance between ring centroids. Angle: Dihedral angle between planes *I* and *J*. Distance 1: Distance between plane *I* and centroid of Cg(*J*). α: Angle between Cg(*I*)-Cg(*J*) vector and normal to plane *I*. Distance 2: Distance between plane *J* and centroid of Cg(*I*). β: Angle between Cg(*J*)-Cg(*I*) vector and normal to plane *J*.

Entry	π-π interactions	Cg-Cg	Angle	Distance 1	α	Distance 2	β
1	Cg1-Cg2d	4.289(3)	23.76(16)	3.778(5)	28.25	3.131(7)	43.11
2	Cg1-Cg3	4.300(3)	44.37(15)	3.560(5)	34.11	4.207(3)	11.94

Table S6. π-π stacking interactions in **2** (distance (Å), angles: (°))**.** Cg-Cg: Distance between ring centroids. Angle: Dihedral angle between planes *I* and *J*. Distance 1: Distance between plane *I* and centroid of Cg(*J*). α: Angle between Cg(*I*)-Cg(*J*) vector and normal to plane *I*. Distance 2: Distance between plane *J* and centroid of Cg(*I*). β: Angle between Cg(*J*)-Cg(*I*) vector and normal to plane *J*.

Entry	π-π interactions	Cg-Cg	Angle	Distance 1	α	Distance 2	β
1	Cg1-Cg2	3.701(4)	6.6(2)	3.395(5)	23.46	3.542(4)	16.86
2	Cg3-Cg4	4.390(4)	25.89(19)	3.518(7)	36.74	3.661(8)	33.49
3	Cg5-Cg6	3.952(4)	9.5(2)	3.645(5)	22.73	3.620(6)	23.65
4	Cg5-Cg7	3.798(4)	14.2(2)	3.360(5)	27.79	3.683(4)	14.14
5	Cg8-Cg9	3.815(4)	8.3(3)	3.166(8)	33.91	3.440(7)	25.62
6	Cg8-Cg10	5.086(5)	31.3(3)	3.523(12)	46.16	3.378(17)	48.38

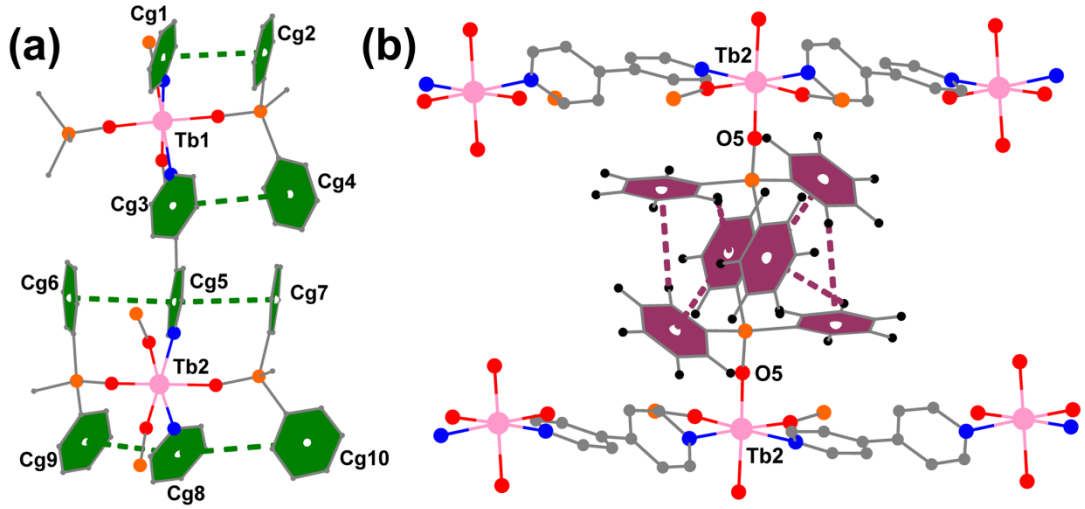

Figure S2 (a) π-π interaction and (b) chain-to-chain C-H...π interactions of complex **2** (dashed line). Color code: pink (Tb), red (O), orange (Si), gray (C), blue (N), black (H).

Table S7. π-π stacking interactions in **3** (distance (Å), angles: (°))**.** Cg-Cg: Distance between ring centroids. Angle: Dihedral angle between planes *I* and *J*. Distance 1: Distance between plane *I* and centroid of Cg(*J*). α: Angle between Cg(*I*)-Cg(*J*) vector and normal to plane *I*. Distance 2: Distance between plane *J* and centroid of Cg(*I*). β: Angle between Cg(*J*)-Cg(*I*) vector and normal to plane *J*.

Entry	π-π interactions	Cg-Cg	Angle	Distance 1	α	Distance 2	β
1	Cg1-Cg2	4.022(7)	25.3(4)	3.866(9)	16.01	3.242(15)	36.29
2	Cg1-Cg3	4.530(8)	51.9(4)	4.506(8)	5.90	2.46(2)	57.11
3	Cg4-Cg5	4.000(7)	32.5(5)	3.152(18)	38.00	3.981(8)	5.59
4	Cg4-Cg6	5.000(8)	50.9(5)	4.472(18)	26.27	1.47(3)	72.90
5	Cg7-Cg8	4.076(9)	24.9(6)	3.887(12)	17.52	3.253(19)	37.05
6	Cg9-Cg10	4.033(7)	32.7(5)	3.178(16)	38.00	4.013(8)	5.71

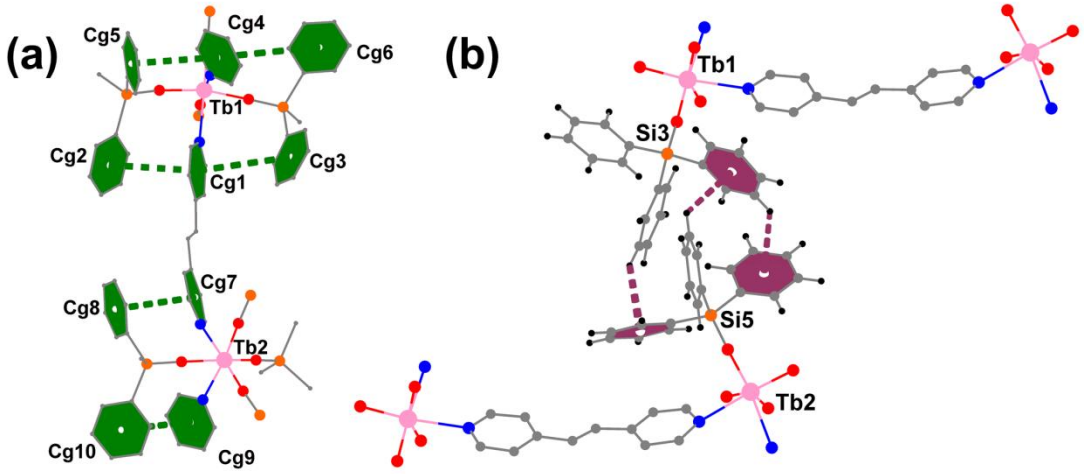

Figure S3 (a) π-π interaction and (b) chain-to-chain C-H...π interactions of complex **3** (black dashed line). Color code: pink (Tb), red (O), orange (Si), gray (C), blue (N), black (H).

Table S8. π-π stacking interactions in **4** (distance (Å), angles: (°))**.** Cg-Cg: Distance between ring centroids. Angle: Dihedral angle between planes *I* and *J*. Distance 1: Distance between plane *I* and centroid of Cg(*J*). α: Angle between Cg(*I*)-Cg(*J*) vector and normal to plane *I*. Distance 2: Distance between plane *J* and centroid of Cg(*I*). β: Angle between Cg(*J*)-Cg(*I*) vector and normal to plane *J*.

Entry	π-π interactions	Cg-Cg	Angle	Distance 1	α	Distance 2	β
1	Cg1-Cg2	3.989(7)	21.6(4)	3.768(9)	19.16	3.259(14)	35.21
2	Cg3-Cg4	4.027(6)	29.8(4)	3.207(14)	37.21	3.992(7)	7.56
3	Cg3-Cg5	4.828(7)	54.1(5)	4.554(12)	19.40	1.50(3)	71.90
4	Cg6-Cg7	4.071(8)	23.0(5)	3.806(11)	20.79	3.228(18)	37.54
5	Cg8-Cg9	4.025(7)	29.5(4)	3.981(8)	8.48	3.199(13)	37.36

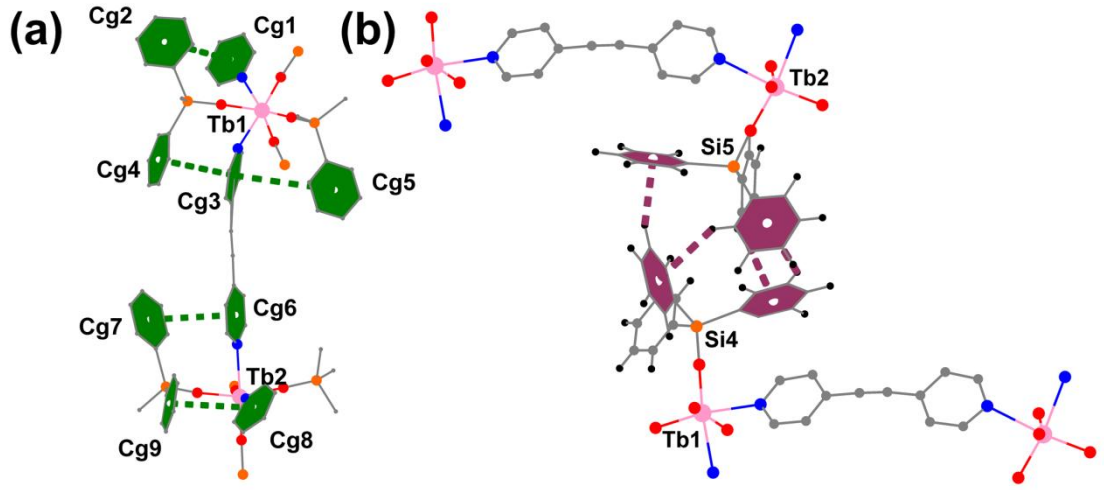

Figure S4 (a) π-π interaction and (b) chain-to-chain C-H...π interactions of complex **4** (black dashed line). Color code: pink (Tb), red (O), orange (Si), gray (C), blue (N), black (H).

Table S9. π-π stacking interactions in **5** (distance (Å), angles: (°))**.** Cg-Cg: Distance between ring centroids. Angle: Dihedral angle between planes *I* and *J*. Distance 1: Distance between plane *I* and centroid of Cg(*J*). α: Angle between Cg(*I*)-Cg(*J*) vector and normal to plane *I*. Distance 2: Distance between plane *J* and centroid of Cg(*I*). β: Angle between Cg(*J*)-Cg(*I*) vector and normal to plane *J*.

Entry	π-π interactions	Cg-Cg	Angle	Distance 1	α	Distance 2	β
1	Cg1-Cg2	3.921(3)	22.89(18)	3.322(5)	32.09	3.847(3)	11.15
2	Cg1-Cg3[c]	4.209(3)	16.78(19)	3.549(6)	32.52	3.382(7)	36.53

4. Hirshfeld surface analysis[21]

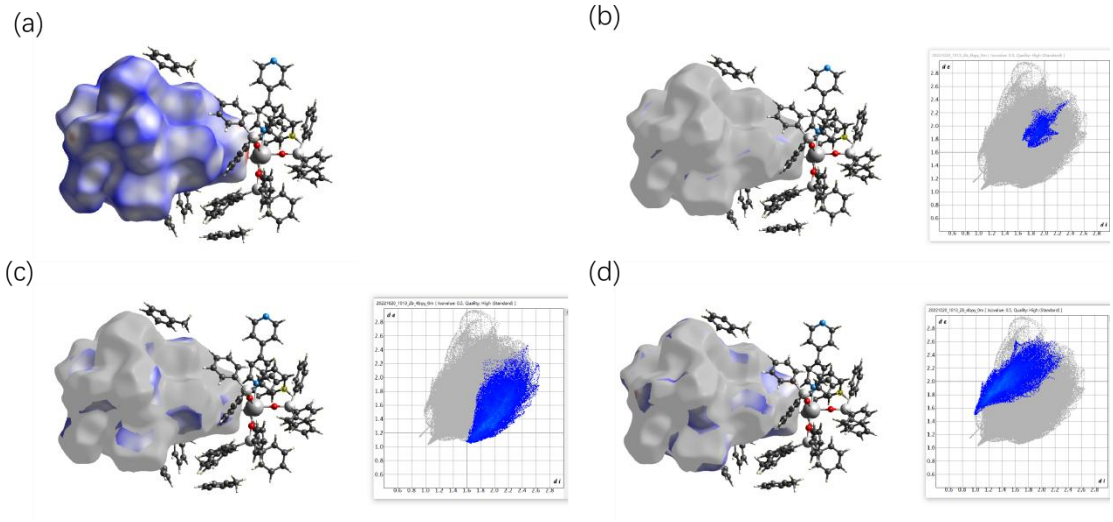

Figure S5. The hirshfeld surface plot maps of **2** (a) and 2D fingerprint plots with [C···C] interaction contributing 2.1% (b), [C···H] interaction contributing 14.7% (c), [H···C] interaction contributing 13.7% (d).

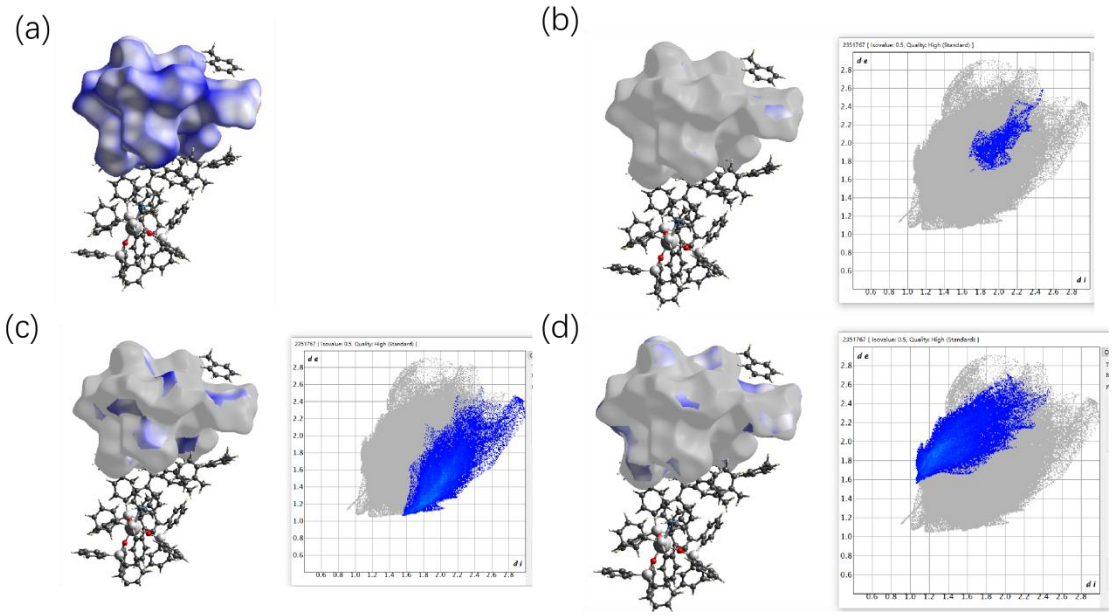

Figure S6. The hirshfeld surface plot maps of **3** (a) and 2D fingerprint plots with [C···C] interaction contributing 1.4% (b), [C···H] interaction contributing 15.5% (c), [H···C] interaction contributing 13.8% (d).

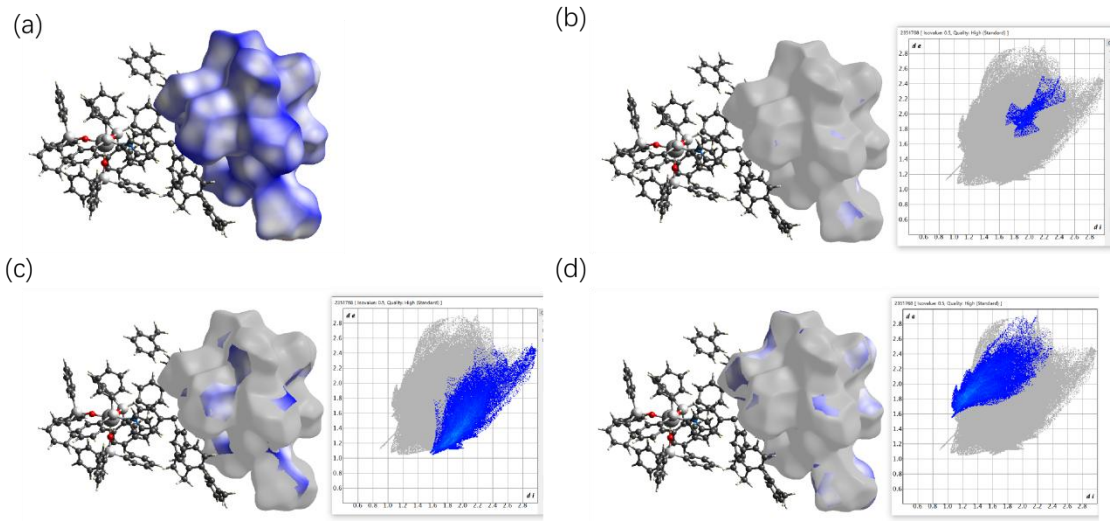

Figure S7. The hirshfeld surface plot maps of **4** (a) and 2D fingerprint plots with [C···C] interaction contributing 1.4% (b), [C···H] interaction contributing 16.3% (c), [H···C] interaction contributing 13.9% (d).

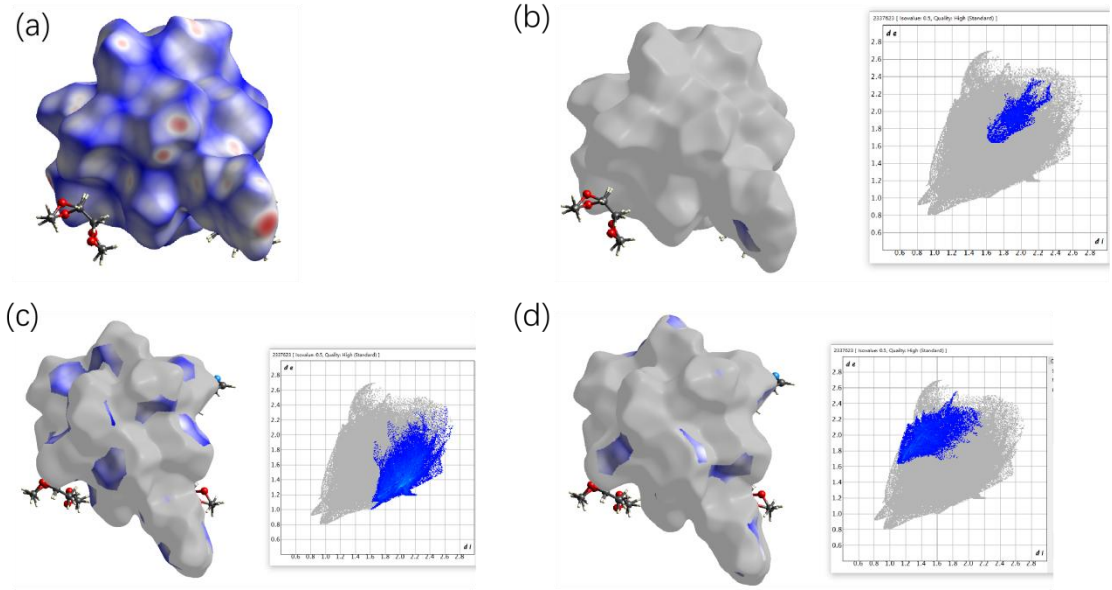

Figure S8. The hirshfeld surface plot maps of **5** (a) and 2D fingerprint plots with [C···C] interaction contributing 1.8% (b), [C···H] interaction contributing 18.7% (c), [H···C] interaction contributing 6.6% (d).

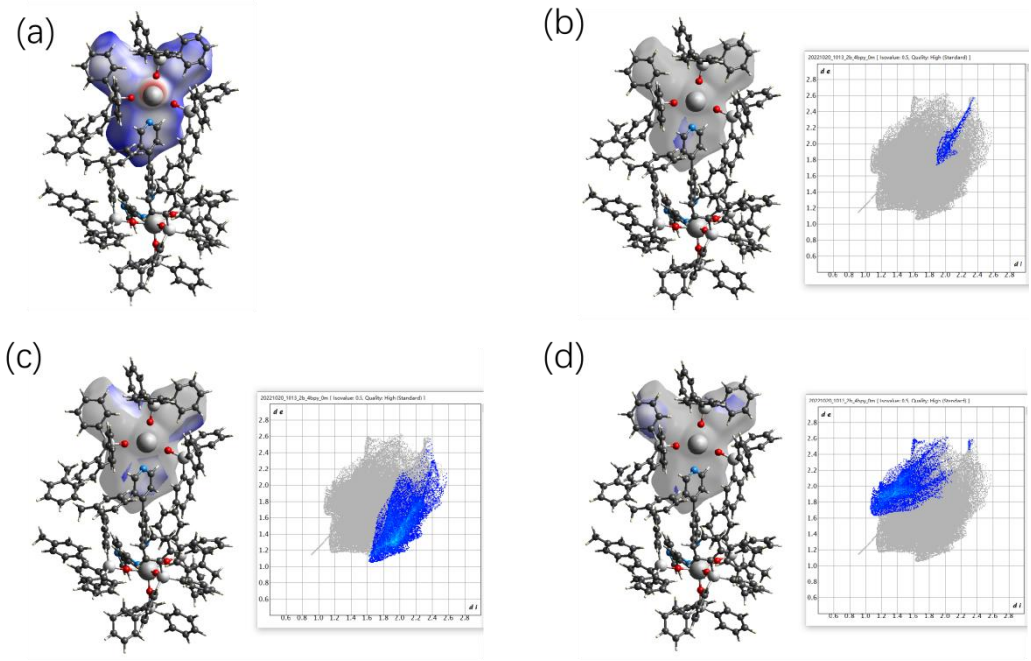

Figure S9. The hirshfeld surface plot maps of Ph_3SiO^- (no. 1) in **2** (a) and 2D fingerprint plots with [C···C] interaction contributing 1.3% (b), [C···H] interaction contributing 19.6% (c), [H···C] interaction contributing 13.8% (d).

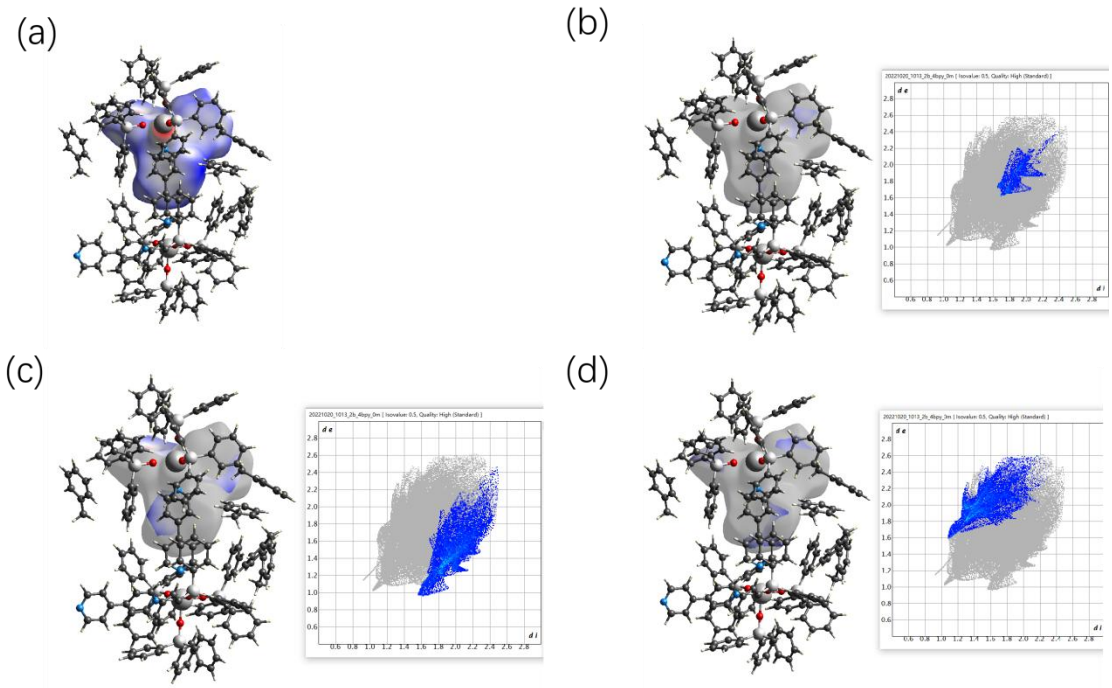

Figure S10. The hirshfeld surface plot maps of Ph_3SiO^- (no. 2) in **2** (a) and 2D fingerprint plots with [C···C] interaction contributing 4.0% (b), [C···H] interaction contributing 16.0% (c), [H···C] interaction contributing 14.9% (d).

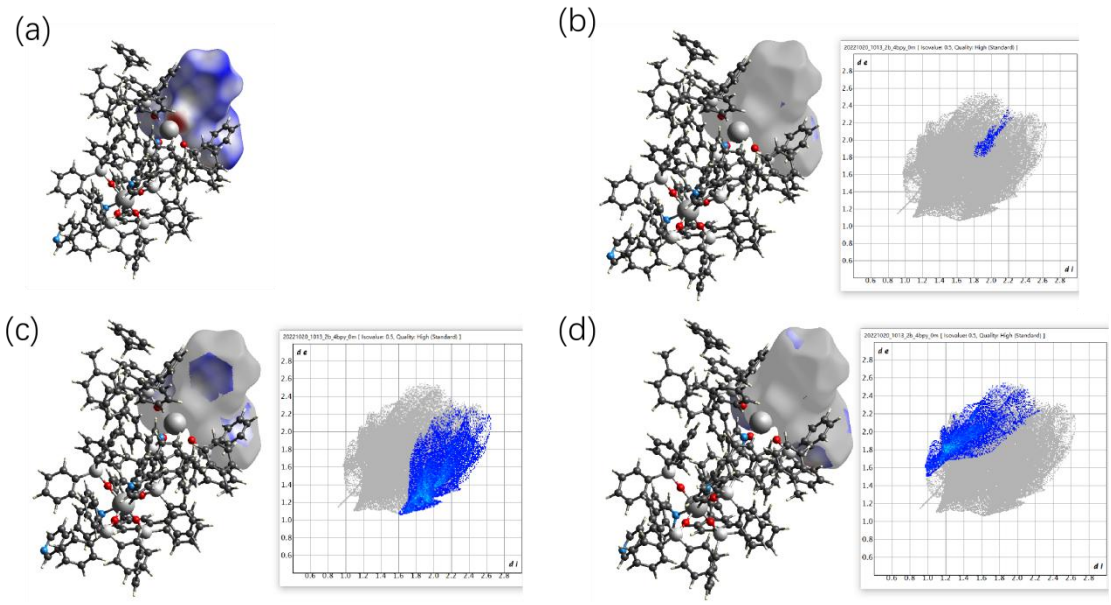

Figure S11. The hirshfeld surface plot maps of Ph_3SiO^- (no. 3) in **2** (a) and 2D fingerprint plots with [C···C] interaction contributing 1.8% (b), [C···H] interaction contributing 18.7% (c), [H···C] interaction contributing 6.6% (d).

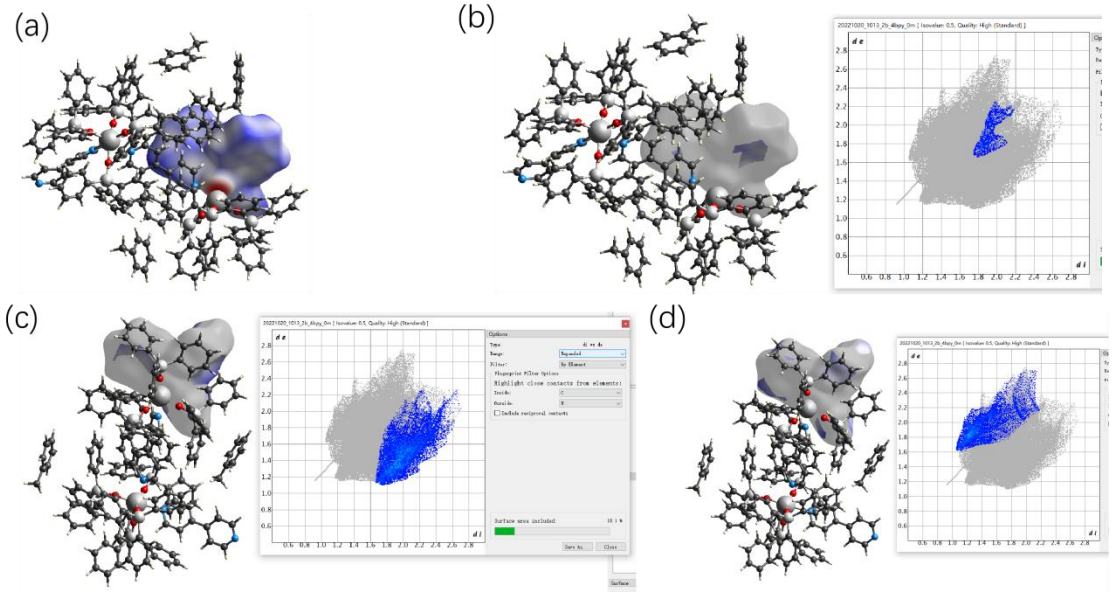

Figure S12. The hirshfeld surface plot maps of Ph_3SiO^- (no. 4) in **2** (a) and 2D fingerprint plots with [C···C] interaction contributing 1.9% (b), [C···H] interaction contributing 18.1% (c), [H···C] interaction contributing 11.6% (d).

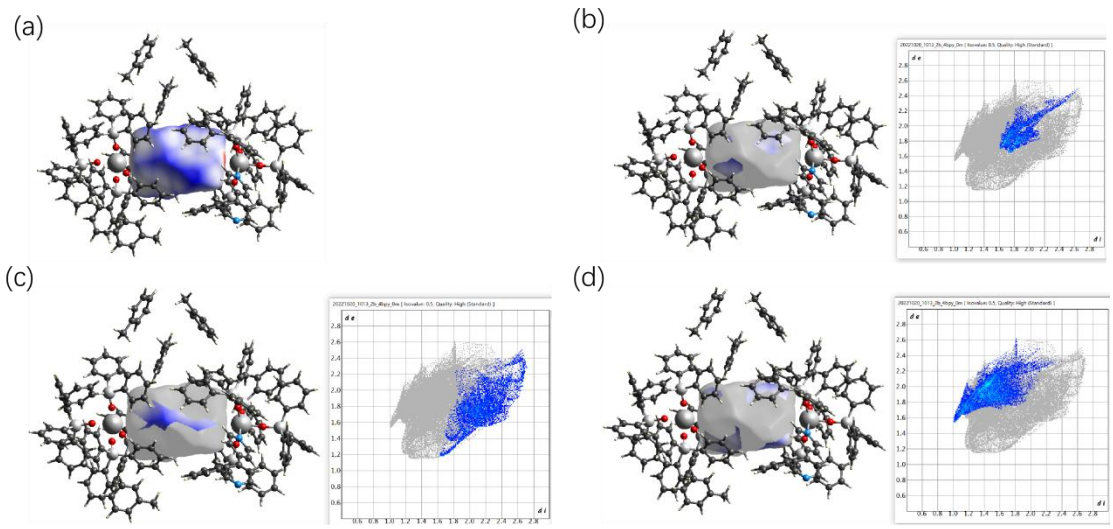

Figure S13. The hirshfeld surface plot maps of **L1** in **2** (a) and 2D fingerprint plots with [C···C] interaction contributing 9.4% (b), [C···H] interaction contributing 18.7% (c), [H···C] interaction contributing 22.6% (d).

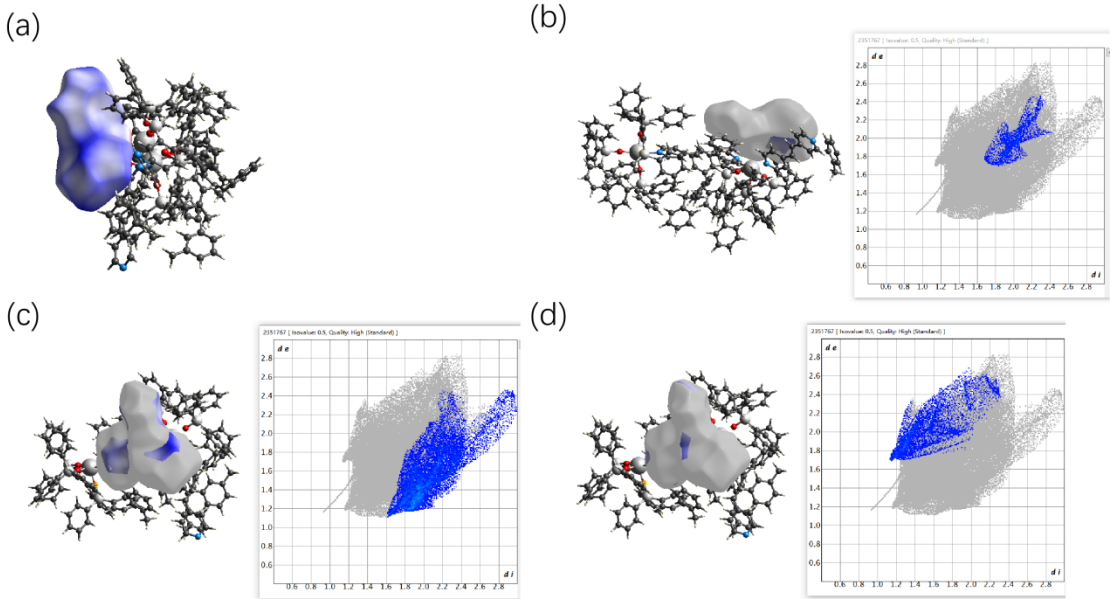

Figure S14. The hirshfeld surface plot maps of Ph_3SiO^- (no. 1) in **3** (a) and 2D fingerprint plots with [C···C] interaction contributing 3.0% (b), [C···H] interaction contributing 17.1% (c), [H···C] interaction contributing 6.5% (d).

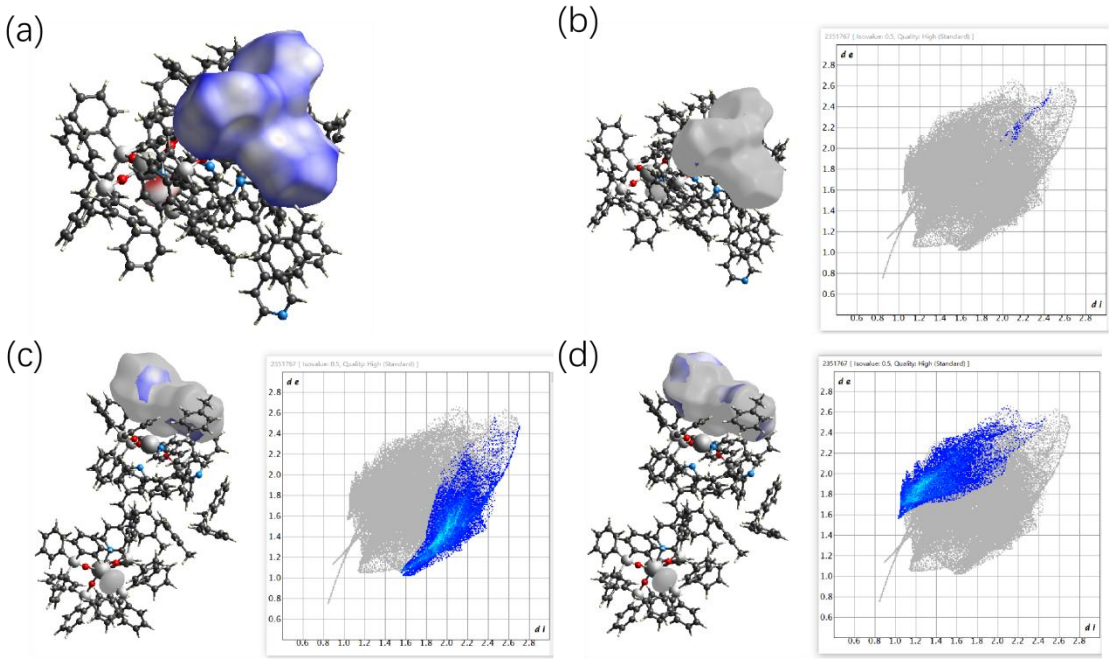

Figure S15. The hirshfeld surface plot maps of Ph_3SiO^- (no. 2) in **3** (a) and 2D fingerprint plots with [C···C] interaction contributing 0.1% (b), [C···H] interaction contributing 20.3% (c), [H···C] interaction contributing 19.0% (d).

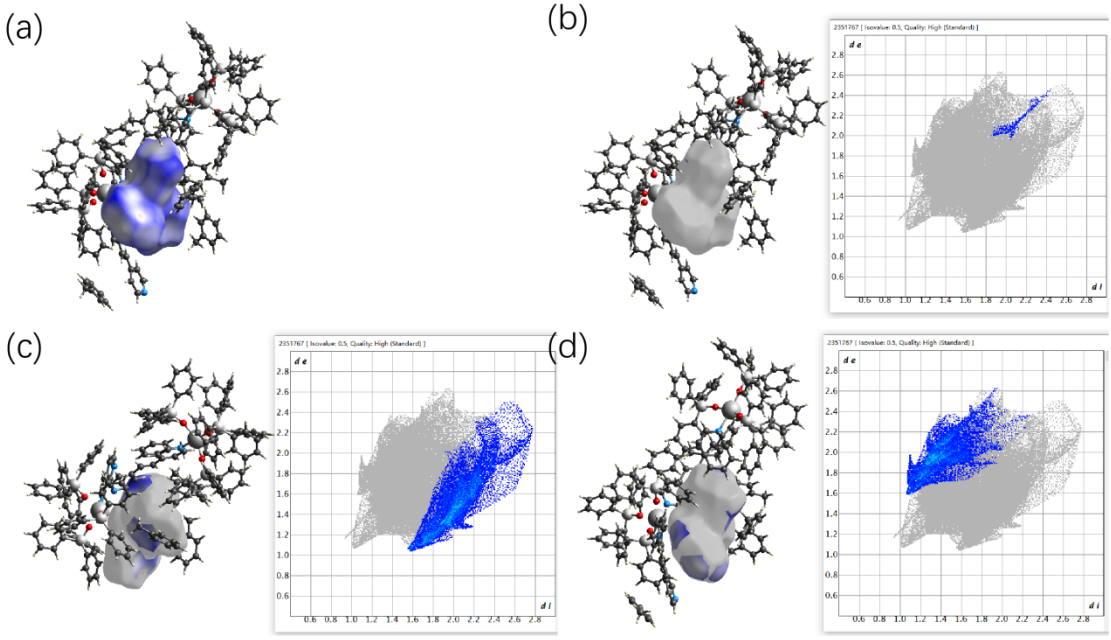

Figure S16. The hirshfeld surface plot maps of Ph_3SiO^- (no. 3) in **3** (a) and 2D fingerprint plots with [C···C] interaction contributing 0.6% (b), [C···H] interaction contributing 19.7% (c), [H···C] interaction contributing 15.2% (d).

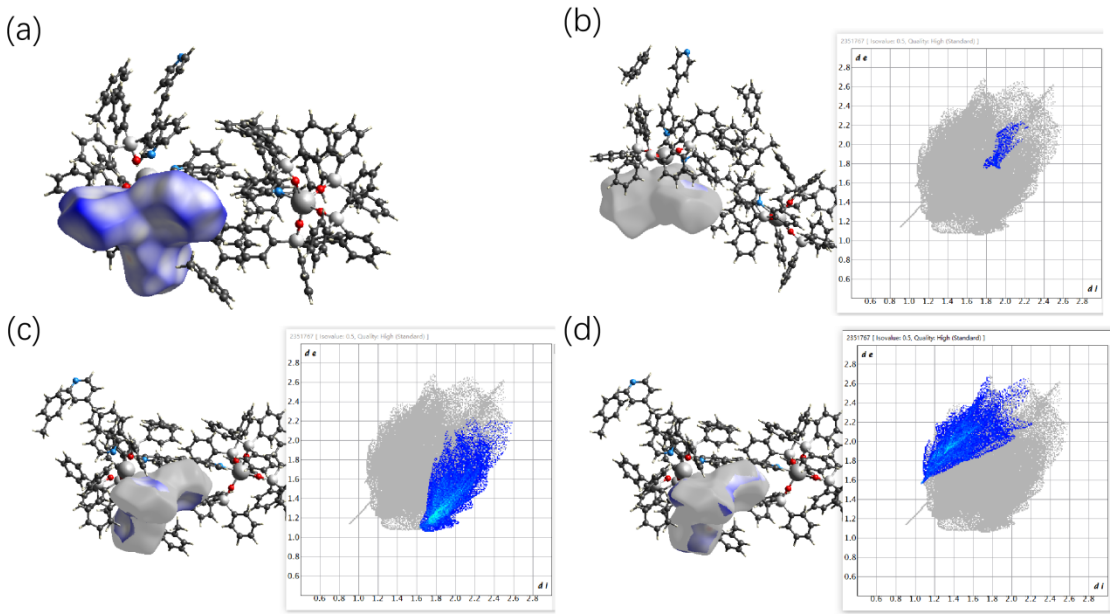

Figure S17. The hirshfeld surface plot maps of Ph_3SiO^- (no. 4) in **3** (a) and 2D fingerprint plots with [C···C] interaction contributing 1.0% (b), [C···H] interaction contributing 20.3% (c), [H···C] interaction contributing 16.5% (d).

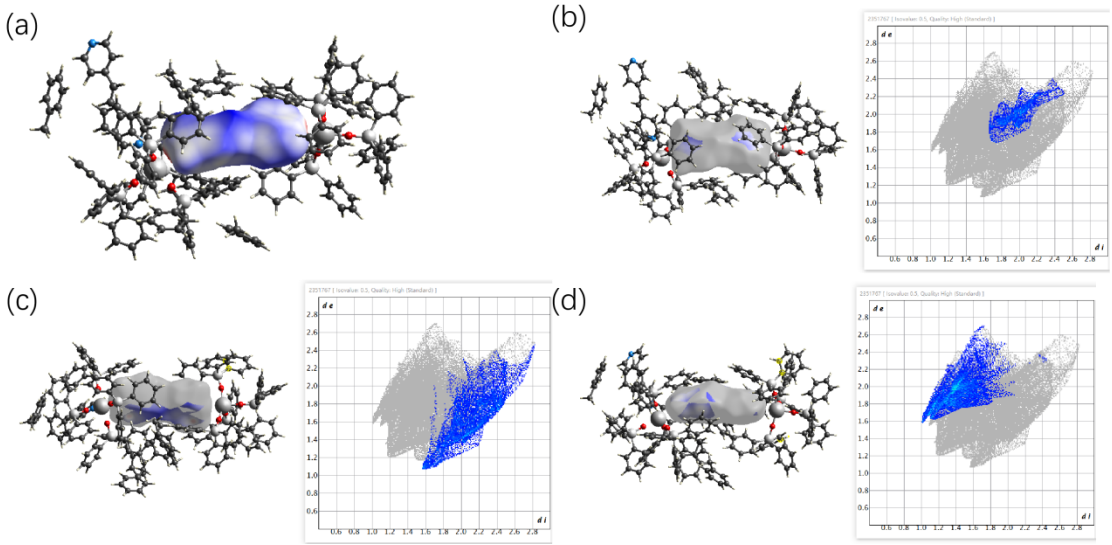

Figure S18. The hirshfeld surface plot maps of **L2** in **3** (a) and 2D fingerprint plots with [C···C] interaction contributing 6.5% (b), [C···H] interaction contributing 18.2% (c), [H···C] interaction contributing 18.9% (d).

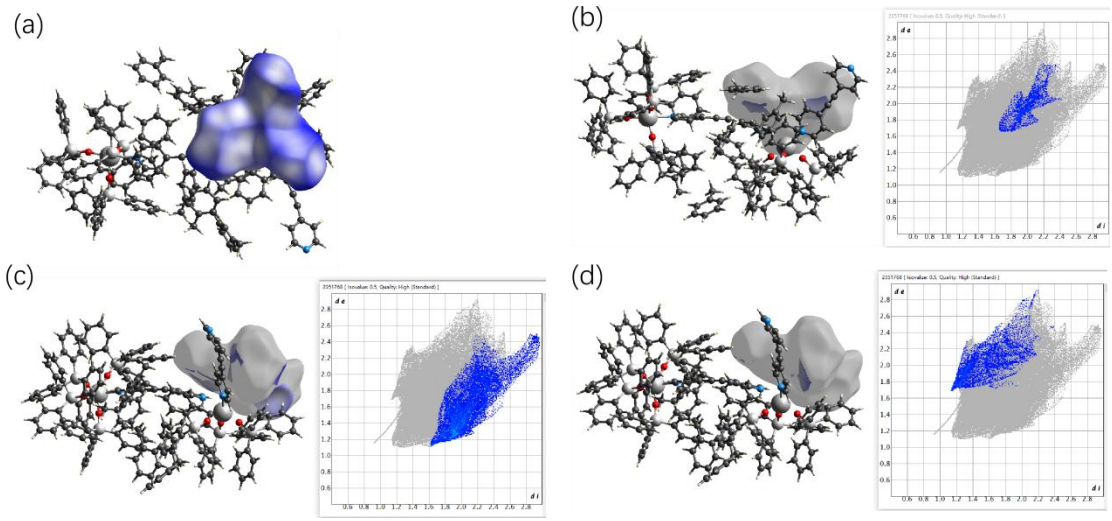

Figure S19. The hirshfeld surface plot maps of Ph_3SiO^- (no. 1) in **4** (a) and 2D fingerprint plots with [C···C] interaction contributing 3.2% (b), [C···H] interaction contributing 16.9% (c), [H···C] interaction contributing 6.6% (d).

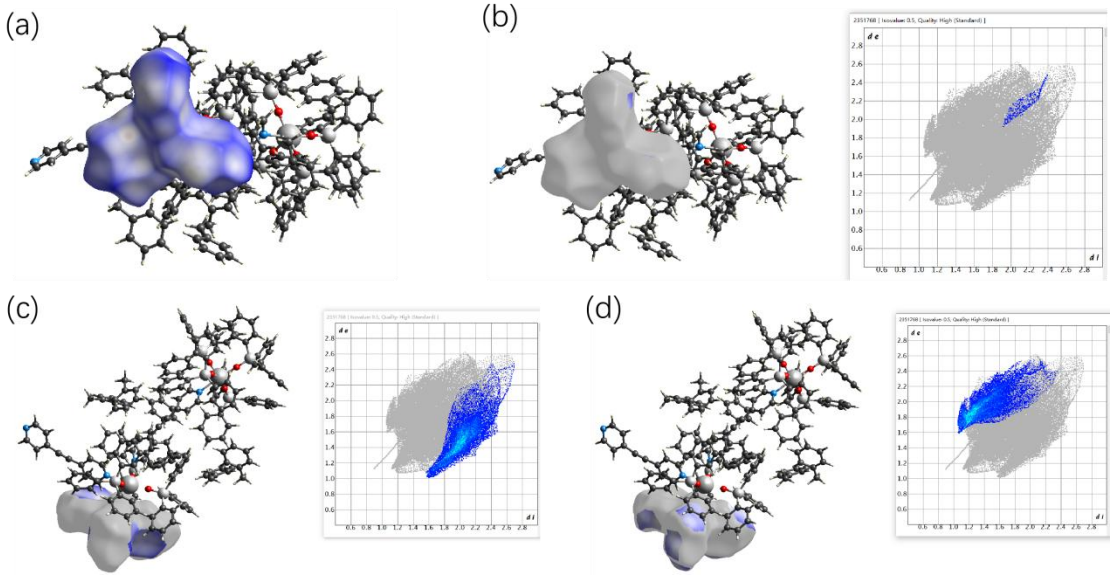

Figure S20. The hirshfeld surface plot maps of Ph_3SiO^- (no. 2) in **4** (a) and 2D fingerprint plots with [C···C] interaction contributing 0.4% (b), [C···H] interaction contributing 21.4% (c), [H···C] interaction contributing 20.1% (d).

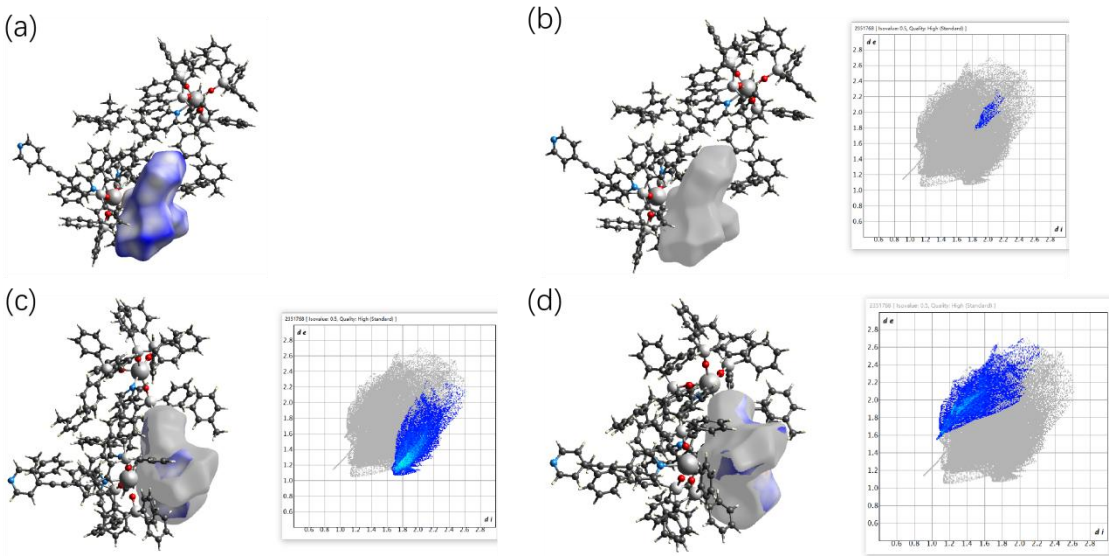

Figure S21. The hirshfeld surface plot maps of Ph_3SiO^- (no. 3) in **4** (a) and 2D fingerprint plots with [C···C] interaction contributing 0.7% (b), [C···H] interaction contributing 20.6% (c), [H···C] interaction contributing 15.3% (d).

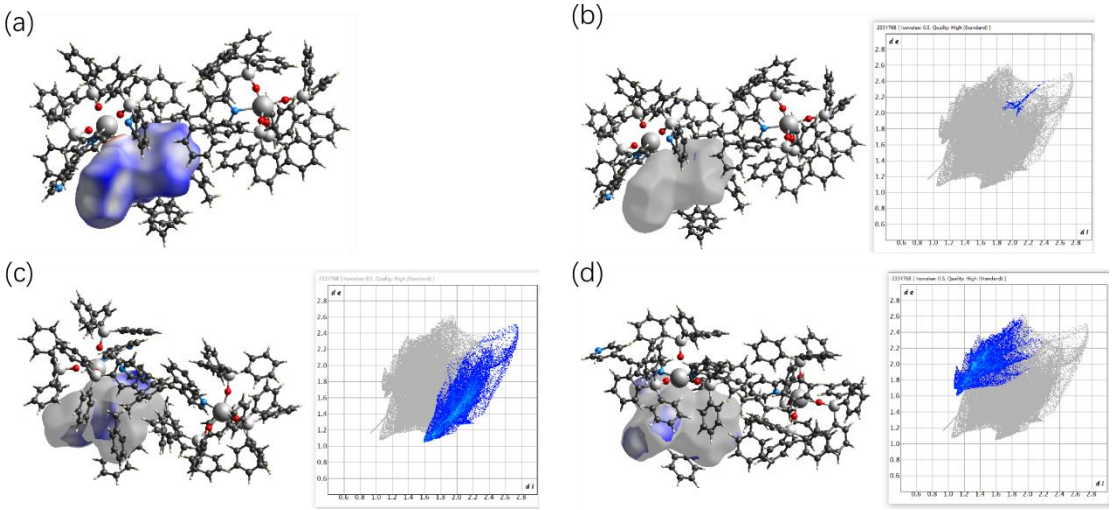

Figure S22. The hirshfeld surface plot maps of Ph_3SiO^- (no. 4) in **4** (a) and 2D fingerprint plots with [C···C] interaction contributing 0.4% (b), [C···H] interaction contributing 19.7% (c), [H···C] interaction contributing 15.6% (d).

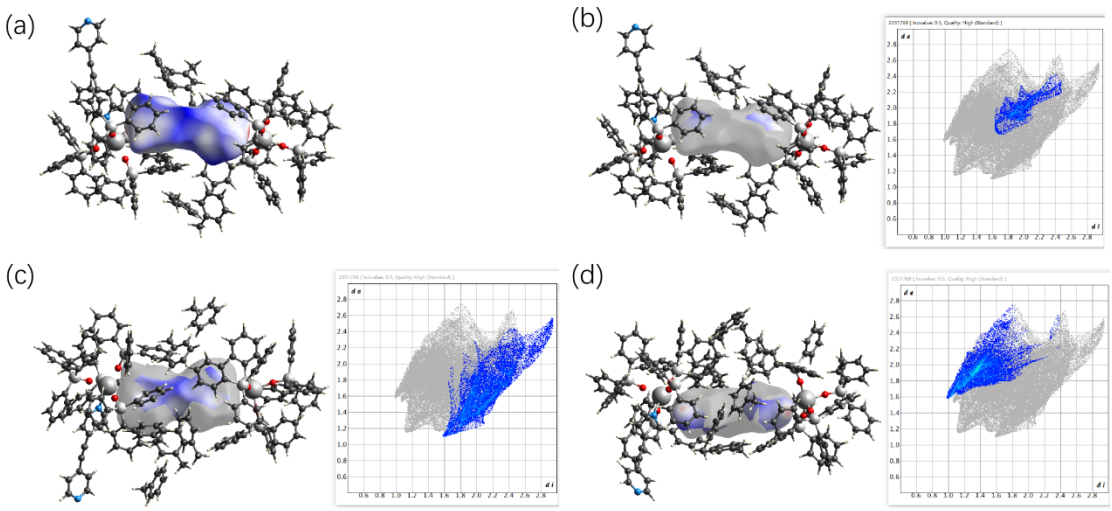

Figure S23. The hirshfeld surface plot maps of **L3** in **4** (a) and 2D fingerprint plots with [C···C] interaction contributing 6.3% (b), [C···H] interaction contributing 23.6% (c), [H···C] interaction contributing 19.6% (d).

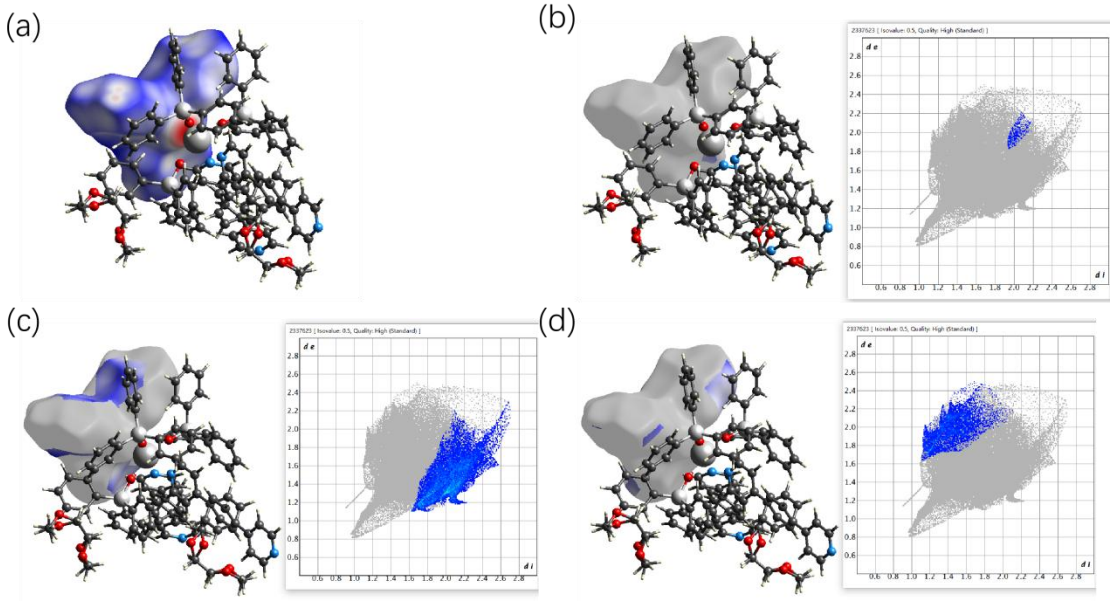

Figure S24. The hirshfeld surface plot maps of Ph_3SiO^- (no. 1) in **5** (a) and 2D fingerprint plots with [C···C] interaction contributing 0.5% (b), [C···H] interaction contributing 21.0% (c), [H···C] interaction contributing 8.1% (d).

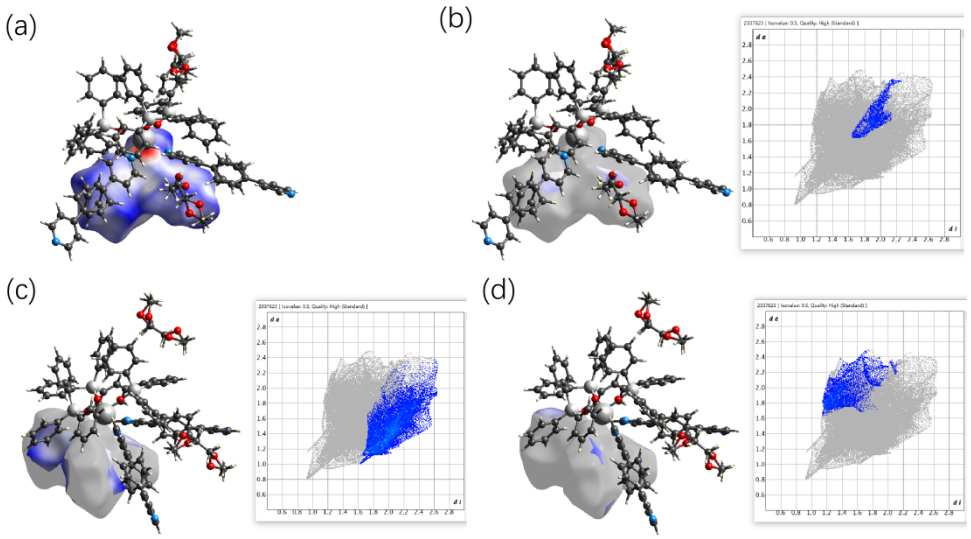

Figure S25. The hirshfeld surface plot maps of Ph_3SiO^- (no. 2) in **5** (a) and 2D fingerprint plots with [C···C] interaction contributing 2.7% (b), [C···H] interaction contributing 18.7% (c), [H···C] interaction contributing 6.6% (d).

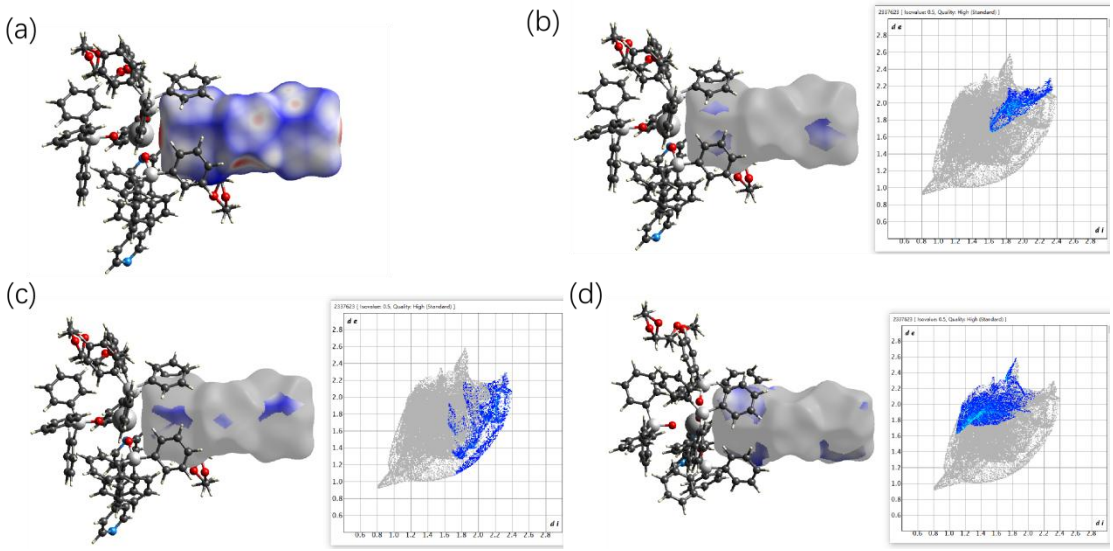

Figure S26. The hirshfeld surface plot maps of **L4** in **5** (a) and 2D fingerprint plots with [C···C] interaction contributing 7.7% (b), [C···H] interaction contributing 7.7% (c), [H···C] interaction contributing 16.5% (d).

Note: there are only two Ph_3SiO^- groups in the asymmetric unit of **5**, so that the hirshfeld surface plot maps of no. 3 and no. 4 Ph_3SiO^- groups coordinated to Tb(IV) ion are identical to no. 1 and no. 2 Ph_3SiO^- groups.

5. Power X-ray diffraction patterns

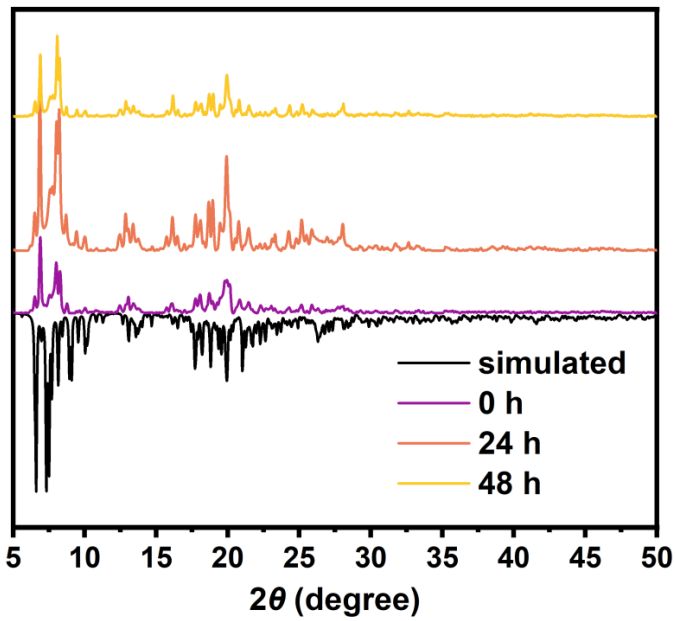

Figure S27 Power X-ray diffraction patterns produced by the pristine coordination polymers **3** and the samples recovered after exposure in air for 24 and 48 hours versus those simulated from the single-crystal structures.

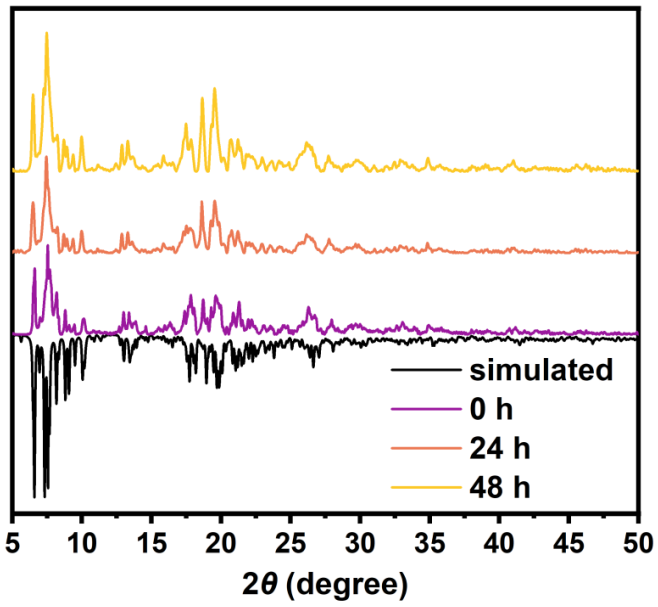

Figure S28 Power X-ray diffraction patterns produced by the pristine coordination polymers **4** and the samples recovered after exposure in air for 24 and 48 hours versus those simulated from the single-crystal structures.

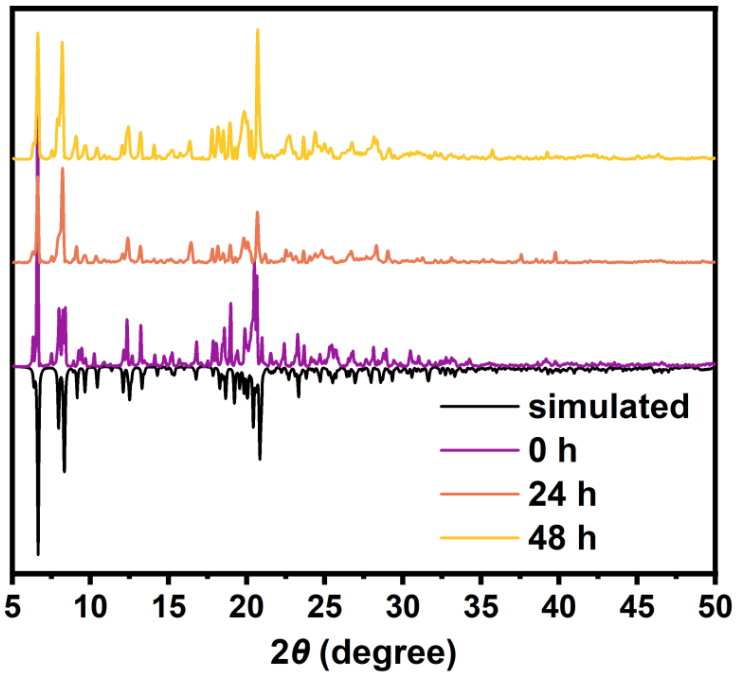

Figure S29 Power X-ray diffraction patterns produced by the pristine coordination polymers **5** and the samples recovered after exposure in air for 24 and 48 hours versus those simulated from the single-crystal structures.

6. Cyclic Voltammetry

Table S10. Electrochemical Data for the Tb(IV/III) Peak Couple of **1** *vs* Fc/Fc^+ (Fc = Ferrocene) in dichloromethane at different sweep rate.

Sweep Rate (V/s)	E_{pc}-1 (V)	E_{pc}-2 (V)	E_{pa}-1 (V)	E_{pa}-2 (V)
0.05	0.158	-0.339	0.265	0.521
0.1	0.137	-0.274	0.292	0.554
0.25	0.119	-0.257	0.301	0.587
0.5	0.093	-0.255	0.344	0.587
1	0.022	-0.306	0.365	0.664

7. Magnetism

Magnetic susceptibility measurements were carried out with a Quantum Design MPMS-3 SQUID magnetometer, with polycrystalline samples sealed with melted eicosane in NMR tubes under a vacuum. Static magnetic susceptibilities were measured under an applied DC field of 1000 Oe upon cooling from 300 K to 2 K. Field-dependent magnetizations of complexes **1-4** were measured at low temperatures with field up to a maximum field of 7 T.

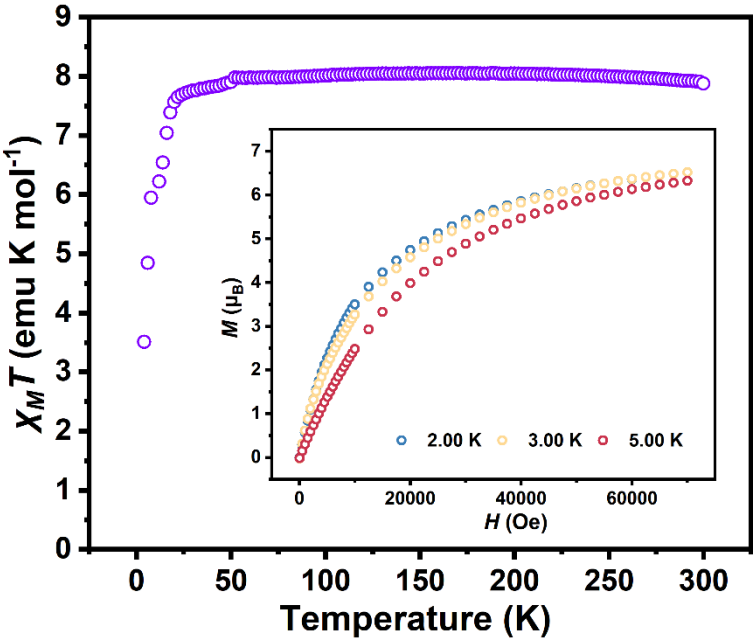

Figure S30. The χT versus T plot of **2** under 1000 Oe dc field (Inset: The field-dependent magnetization plots at 2, 3, and 5 K).

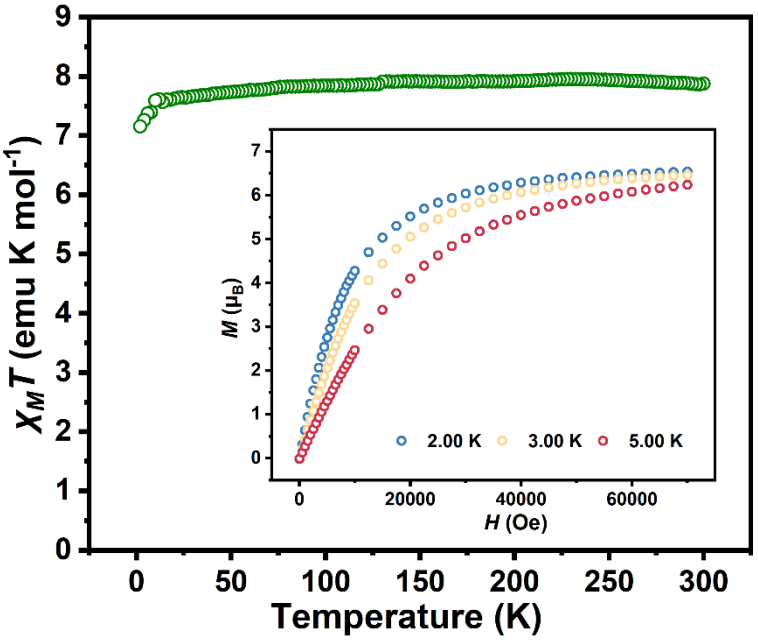

Figure S31. The χT versus T plot of **4** under 1000 Oe dc field (Inset: The field-dependent magnetization plots at 2, 3, and 5 K).

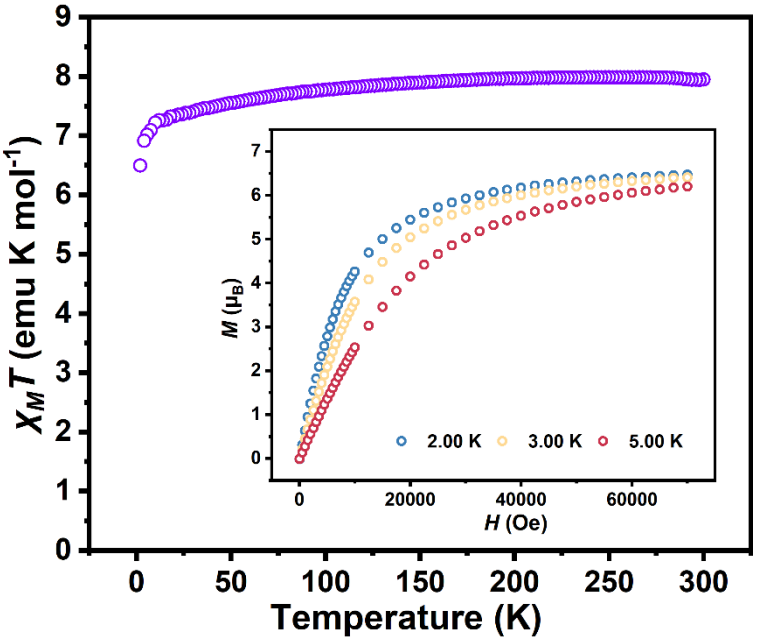

Figure S32. The χT versus T plot of **5** under 1000 Oe dc field (Inset: The field-dependent magnetization plots at 2, 3, and 5 K).

8. Reference

1. Palumbo, C. T.; Zivkovic, I.; Scopelliti, R.; Mazzanti, M. *J. Am. Chem. Soc.* **2019,** *141* (25), 9827-9831.

2. Rice, N. T.; Popov, I. A.; Russo, D. R.; Bacsa, J.; Batista, E. R.; Yang, P.; Telser, J.; La Pierre, H. S. *J. Am. Chem. Soc.* **2019,** *141* (33), 13222-13233.

3. Willauer, A. R.; Palumbo, C. T.; Scopelliti, R.; Zivkovic, I.; Douair, I.; Maron, L.; Mazzanti, M. *Angew. Chem. Int. Ed.* **2020,** *59* (9), 3549-3553.

4. Willauer, A. R.; Douair, I.; Chauvin, A.-S.; Fadaei-Tirani, F.; Bünzli, J.-C. G.; Maron, L.; Mazzanti, M. *Chem. Sci.* **2022,** *13* (3), 681-691.

5. Tricoire, M.; Hsueh, F.-C.; Keener, M.; Rajeshkumar, T.; Scopelliti, R.; Zivkovic, I.; Maron, L.; Mazzanti, M. *Chem. Sci.* **2024**, *15* (18), 6874-6883.

6. Xue, T.; Ding, Y.-S.; Jiang, X.-L.; Tao, L.; Li, J.; Zheng, Z. *Precis. Chem.* **2023,** *1* (10), 583–591.

7. Willauer, A. R.; Palumbo, C. T.; Fadaei-Tirani, F.; Zivkovic, I.; Douair, I.; Maron, L.; Mazzanti, M. *J. Am. Chem. Soc.* **2020**, *142* (12), 5538-5542.

8. Rice, N. T.; Popov, I. A.; Carlson, R. K.; Greer, S. M.; Boggiano, A. C.; Stein, B. W.; Bacsa, J.; Batista, E. R.; Yang, P.; La Pierre, H. S., *Dalton Trans.* **2022,** *51* (17), 6696-6706.

9. Boggiano, A. C.; Chowdhury, S. R.; Roy, M. D.; Bernbeck, M. G.; Greer, S. M.; Vlaisavljevich, B.; La Pierre, H. S. *Angew. Chem. Int. Ed.* **2024**, *63*, e202409789.

10. Xue, T.; Ding, Y.-S.; Zheng, Z. *Dalton Trans.* **2024,** *53*, 5779-5783.

11. Boggiano, A. C.; Studvick, C. M.; Chowdhury, S. R.; Niklas, J. E.; Tateyama, H.;

Wu, H.; Leisen, J. E.; Kleemiss, F.; Vlaisavljevich, B.; Popov, I. A.; La Pierre H. S. *ChemRxiv*. **2024**; doi:10.26434/chemrxiv-2024-cb3zj.

12. Huang, W.; Upton, B. M.; Khan, S. I.; Diaconescu,P. L. *Organometallics* **2013,** *32* (5), 1379-1386.

13. McGeary, M. J.; Coan, P. S.; Folting, K.; Streib, W. E.; Caulton, K. G. *Inorg. Chem.* **1991,** *30* (8), 1723-1735.

14. Boduszek, B.; Shine, H. J. *J. Org. Chem.* **1988,** *53* (21), 5142-5143.

15. M. Sevvana, M. Ruf, I. Usón, G. M. Sheldrick and R. Herbst-Irmer, *Acta Crystallogr. D Struct. Bio.l*, 2019, **75**, 1040-1050.

16. P. van der Sluis and A. L. Spek, *Acta Crystallogr. Sect. A*, 1990, **46**, 194-201.

17. Dolomanov, O. V.; Bourhis, L. J.; Gildea, R. J.; Howard, J. A. K.; Puschmann, H. *J. Appl. Crystallogr.* **2009,** *42* (2), 339-341.

18. Sheldrick, G. M. *Acta Crystallogr. Sect. A* **2015,** *71* (1), 3-8.

19. Sheldrick, G. M., *Acta Crystallogr. Sect. C* **2015**, *71*, 3-8.

20. Alvarez, S.; Avnir, D.; Llunell, M.; Pinsky, M. *New J. Chem.* **2002,** *26* (8), 996-1009.

21. P. R. Spackman, M. J. Turner, J. J. McKinnon, S. K. Wolff, D. J. Grimwood, D. Jayatilaka and M. A. Spackman, *J. Appl. Crystallogr.*, 2021, **54**, 1006-1011.